Journal of Solid State Chemistry **149,** 314–319 (2000)
doi:10.1006/jssc.1999.8532, available online at http://www.idealibrary.com on IDEAL®

Hydrothermal Synthesis and Characterization of $Bi_2Pb_2O_7$ with Pyrochlore Structure

Yachun Mao, Guangshe Li, Yinyong Sun, and Shouhua Feng[1]

Key Laboratory of Inorganic Synthesis and Preparative Chemistry, Jilin University, Changchun 130023, People's Republic of China

Received August 4, 1999; in revised form October 5, 1999; accepted October 11, 1999

Pyrochlore $Bi_2Pb_2O_7$ was fabricated under low-temperature hydrothermal conditions and characterized by XRD, IR, SEM DTA–TG, and XPS. XRD analysis shows that the structure of $Bi_2Pb_2O_7$ is cubic, which is similar to that obtained from high-pressure reactions. XPS measurements suggest that the valences of Bi and Pb ions are +3 and +4, respectively. The cubic $Bi_2Pb_2O_7$ is a metastable phase; it decomposes into a new phase with liberation of O_2 at 450°C. © 2000 Academic Press

INTRODUCTION

Bismuth-oxide-based materials are of great importance for their potential application as solid electrolytes (1, 2). However, it is very difficult to obtain single-phase products from the binary system Bi_2O_3–PbO_2 under the normal pressure during traditional solid–state reactions, because of the volatility of PbO from the decomposition of PbO_2 during the calcination (3). High-pressure, such as a pressure of 3000 MPa, was critical for the synthesis of oxides $A_2Pb_2O_7$, A = Tl, and Bi (4), which to some degree limited the studies on the properties of these materials. Moreover, conventional ceramic methods require multiple steps of mixing, grinding, and firing of the component oxides or carbonates at high temperatures. This has many drawbacks, notably the major problems of air pollution and energy consumption. Therefore, there is a great need to develop convenient and inexpensive mild chemistry routes to complex oxides (5, 6).

Low-temperature hydrothermal reactions have yielded a large number of novel inorganic compounds, including complex oxides and fluorides (7–13), which are very hard to prepare by conventional solid-state reactions. With the aim of developing a mild route to novel compounds without complicated synthesis procedures, we continue our previous work on the bismuth-containing hydrothermal systems (8, 10, 11). Here, we report the hydrothermal stabilization and thermal behavior of a high-pressure phase, $Bi_2Pb_2O_7$.

[1]To whom correspondence should be addressed.

EXPERIMENTAL

Sample Synthesis

During the synthesis of $Bi_2Pb_2O_7$, $Pb(NO_3)_2$, PbO, PbO_2, $NaBiO_3$, $Bi(NO_3)_3$, and NaOH were used as the starting reactants. In comparison with the solid-state reactions, the present hydrothermal synthesis is relatively simple. A typical synthesis procedure for $Pb_2Bi_2O_7$ was 1.35 g $Pb(NO_3)_2$ and 1.28 g $NaBiO_3$ were mixed with 25 ml 1 mol/L NaOH solution to form a reaction mixture. The reaction mixture was sealed in a Teflon-lined stainless-steel autoclave and allowed to crystallize at 140–240°C for 1–3 days under autogenous pressure. Crystalline products were filtered, washed with distilled water, and dried at room temperature.

Chemical Analysis

The sample was weighted accurately and then dissolved in an HCl (6 mol/L) solution in the presence of excess H_2O_2 at 100°C, where Pb^{IV} was reduced to Pb^{II}. Bi^{III} was titrated with EDTA (0.02 mol/L) solution in an acidic medium (0.1 mol/L HCl) using XO as the indicator. The pH of the solution was adjusted to 6 with hexamine buffer solution. Titration was carried out with an EDTA (0.02 mol/L) solution to determine the content of Pb.

The average valences of Pb and Bi were determined according to a previous reference (14). The sample was dissolved in HCl (6 mol/L) solution containing KI. Iodine was liberated by reactions

$$Bi^{5+} + 2I^- \rightarrow Bi^{3+} + I_2 \qquad [1]$$

$$Pb^{4+} + 4I^- \rightarrow PbI_2 + I_2. \qquad [2]$$

The content of iodine was determined by using 0.1 N $Na_2S_2O_3$ solution. In the experiment, 2 mol of I^- were

0022-4596/00 $35.00

oxidized for each molar of the product. Therefore, the sum valence of Pb and Bi ions is 7.

Sample Characterization

All powder products were identified by means of X-ray diffraction on a Riguku D/max-A, 12Kw XRD diffractiometer with a rotating target and Ni-filtered Cu$K\alpha$ radiation. A 2θ scan was employed to collect the diffraction data with a step of 0.02°, Silicon powder (99.99% purity) was used as an internal standard for peak position determination. The lattice parameters for the samples were determined by the least-square method.

The valence states of bismuth and lead in the samples were detected by X-ray photoelectron spectroscopy (XPS) on an ESCA-LAB MKII X-ray photoelectron spectrometer from the VG Co. with Al$K\alpha$ radiation. The base pressure was 10^{-7} Pa. A C 1*s* signal was used to correct the charge effects.

A scanning electron micrograph (SEM) of the sample was taken with a Hitachi X-650B electron microscope. The infrared (IR) spectrum was recorded by a Nicolet 5DX FTIR instrument with a KBr pellet technique. Inductively coupled plasma analysis (ICP) was carried out for chemical analysis of the product on a POEMS ICP instrument. Differential thermal analysis (DTA) and thermal gravimetric analysis (TG) were performed on a Perkin–Elmer 7000 differential thermal analyzer and a TG-7 thermogravimetric analyzer. The sample was heated and cooled at a heating rate of 10°C min^{-1} in a 1 atom O_2 gas flow.

In electrical measurements, powder samples were pressed into a compact (6 mm in diameter and 2 mm thick) under a pressure of 12 MPa. The ionic conductivity measurements were performed by an ac complex impedance method at frequencies ranging from 5 Hz to 1 MHz using a Solarton 1260A impedance/gain-phase analyzer.

RESULTS AND DISCUSSION

1. Effects of the Reactant Sources on the Crystallization of $Bi_2Pb_2O_7$

For the Bi_2O_3–PbO_2 hydrothermal systems, the product formation was dependent upon the types of the reactants, as shown in Table 1. The use of Bi $(NO_3)_3$ and PbO_2 as the Bi ad Pb sources led to a relatively simple reaction from the point of view of oxidation state changes from the reactants to products. In an alternative synthesis, $NaBiO_3$ and $Pb(NO_3)_2$ were found to be the suitable starting reagents for $Bi_2Pb_2O_7$ due to their soluble characteristics. When $NaBiO_3$ reacted with PbO or $Pb(NO_3)_2$, $Bi_2Pb_2O_7$ could also be obtained, but we believe that the reaction procedure was more complicated. In such a reaction system, a redox reaction might occur:

TABLE 1
The Effect of the Types of Starting Reactants on the Formation of $Bi_2Pb_2O_7$

Lead source	Bismuth source	Product phase
PbO_2	$Bi(NO_3)_3$	$Bi_2Pb_2O_7$
PbO	$NaBiO_3$	$Bi_2Pb_2O_7$
$Pb(NO_3)_2$	$NaBiO_3$	$Bi_2Pb_2O_7$
PbO_2	$NaBiO_3$	$Bi_2Pb_2O_7$
PbO	$Bi(NO_3)_3$	impurity
$Pb(NO_3)_2$	$Bi(NO_3)_3$	impurity

$$2NaBi^{5+}O_3 + 2Pb^{2+}O + H_2O \rightarrow Bi_2^{3+}Pb_2^{4+}O_7 + 2OH^- + 2Na^+$$

$$2NaBi^{5+}O_3 + 2Pb^{2+}(NO_3)_2 + 2OH^- \rightarrow Bi_2^{3+}Pb_2^{4+}O_7 + H_2O + 2Na^+ + 4NO_3^-.$$

When PbO_2 and $NaBiO_3$ were used as the starting materials, single-phase $Bi_2Pb_2O_7$ could also be obtained, even though no reductant was involved. The possible reason for the existence of Bi(III) in the products may be some impurity Bi(IV) present in the reactant $NaBiO_3$. Such a redox reaction might exist:

$$2NaBi^{5+}O_3 + 2Pb^{4+}O_2 + H_2O \rightarrow Bi_2^{3+}Pb_2^{4+}O_7 + O_2\uparrow + 2OH^- + 2Na^+.$$

We also examined the structural characteristics of the PbO–Bi_2O_3 hydrothermal systems in which PbO and $Bi(NO_3)_3$ were used as the reactants. No crystallized $Bi_2Pb_2O_7$ was obtained, which may be due to the lack of oxidants in the reaction systems.

2. Effects of pH, Crystallization Temperature, and Time on the Crystallization

The pH value of the reaction mixture, the crystallization temperature, and the reaction time influence the formation of $Bi_2Pb_2O_7$. In a typical synthetic system in which $Pb(NO_3)_2$ and $NaBiO_3$ were used as the reactants, the effects of pH, crystallization temperature, and time on the formation of $Bi_2Pb_2O_7$ were examined (Table 2). Single-phase $Bi_2Pb_2O_7$ could also be obtained under the following conditions: crystallization temperature varying from 140 to 240°C, crystallization time longer than 1 day, and NaOH concentration greater than 1 M.

TABLE 2
Synthesis Conditions for $Bi_2Pb_2O_7$[a]

Starting reactants and their ratios (in mol)	NaOH (in mol)	Crystallization Temp (°C)	Crystallization Time (days)	Product
$Pb(NO_3)_2:NaBiO_3 = 1:1$	3	240	3	$Bi_2Pb_2O_7$
$Pb(NO_3)_2:NaBiO_3 = 1:1$	1	240	3	$Bi_2Pb_2O_7$
$Pb(NO_3)_3:NaBiO_3 = 1:1$	1	140	3	$Bi_2Pb_2O_7$
$Pb(NO_3)_2:NaBiO_3 = 1:1$	1	140	1	$Bi_2Pb_2O_7$
$Pb(NO_3)_2:NaBiO_3 = 1:1$	0.5	140	1	amorphous
$Pb(NO_3)_2:NaBiO_3 = 1:1$	0.5	140	3	amorphous
$Pb(NO_3)_2:NaBiO_3 = 1:1$	0.5	140	7	amorphous
$Pb(NO_3)_2:NaBiO_3 = 1:1$	0.5	240	1	amorphous
$Pb(NO_3)_2:NaBiO_3 = 1:1$	0.5	240	3	amorphous
$Pb(NO_3)_2:NaBiO_3 = 1:1$	0.5	240	7	amorphous
$Pb(NO_3)_2:NaBiO_3 = 1:1$	1	120	1	amorphous
$Pb(NO_3)_2:NaBiO_3 = 1:1$	3	120	1	amorphous
$Pb(NO_3)_2:NaBiO_3 = 1:1$	6	120	1	amorphous
$Pb(NO_3)_2:NaBiO_3 = 1:1$	6	120	3	amorphous
$Pb(NO_3)_2:NaBiO_3 = 1:1$	6	120	7	amorphous
$Pb(NO_3)_2:NaBiO_3 = 1:1$	1	140	0.5	amorphous
$Pb(NO_3)_2:NaBiO_3 = 1:1$	3	140	0.5	amorphous
$Pb(NO_3)_2:NaBiO_3 = 1:1$	6	140	0.5	amorphous
$Pb(NO_3)_2:NaBiO_3 = 1:1$	1	240	0.5	amorphous
$Pb(NO_3)_2:NaBiO_3 = 1:1$	3	240	0.5	amorphous
$Pb(NO_3)_2:NaBiO_3 = 1:1$	6	240	0.5	amorphous

[a] $Pb(NO_3)_2$ and $NaBiO_3$ were used as the lead and the bismuth source, respectively.

3. *Microstructural Characterization and Valence Determination*

The powder XRD pattern for the single-phase product $Bi_2Pb_2O_7$ recorded at room temperature is showed in Fig. 1a. Analysis of the XRD data clearly shows that $Bi_2Pb_2O_7$ crystallizes in a cubic pyrochlore system with a cell parameter of $a = 1.1007(3)$ nm, which is very close to that prepared by the high-pressure reactions ($a = 1.101$ nm) (4). The broad and weak peaks observed in Fig. 1a (*hkl*, all odd, e.g., (511), (551), (731), etc.) are produced by the superlattice with a double cell in comparison with the standard fluorite structures (0.54 nm). Consistently, Hyde (15) has shown that pyrochlore can be described as a defect fluorite with one-eighth of its anion sites unoccupied. Our $Bi_2Pb_2O_7$ sample is a red powder. The morphology of the sample was examined by SEM at room temperature. The uniform grain texture of the product was observed, and the average grain size was ca. 0.3 μm. The IR spectrum of $Bi_2Pb_2O_7$ did not show any strong absorption bands at 1400 or 3500 cm^{-1}, implying traces of CO_3^{2-} of OH^- in the product. This result is different from that reported by Kumada *et al.* on the hydrothermally synthesized alkaline earth pyrochlores, $(A_xBi^{2+}_{y-2}\square_{4-x-y})(Bi^{3+}, Bi^{5+})_2O_{7-3\delta}(CO_3)$ with $A = Ca$ and Sr (16). Compositional analysis of $Bi_2Pb_2O_7$ measured by ICP corresponds to a molar ratio of Pb/Bi = 1:1.

Figure 2 shows the C 1*s* and O 1*s* XPS spectra for $Bi_2Pb_2O_7$. We have noted that, during the XPS measurements, surface species usually influence the analysis of the experimental data, especially for the insulating compounds. The weak C 1*s* peak observed in Fig. 2 is associated with contaminated carbon (300.8 eV) (17). For the insulating compounds, charge effects may result in the increase of the binding energy of the C 1*s* level from the usual contamination. Therefore, for the present work, the C 1*s* signal (284.6 eV) was used as the standard to calibrate the binding energy. The O 1*s* level, as shown in Fig. 2, exhibits two peaks. The peak with lower binding energy (529.5 eV) is assigned to the lattice oxygen. This line occupies the large peak area of the O 1*s* peak, which indicates that our sample has a clean surface. The weaker O 1*s* peak with higher binding energy (532.1 eV) is ascribed to the absorbed oxygen species or hydroxyl group on the sample surface (17).

Figure 3 shows the core-level spectrum of $Bi_2Pb_2O_7$ measured in the Bi 4*f* region. The Bi 4*f* peaks are typical of broad doublets. The fitting results clearly show that both Bi

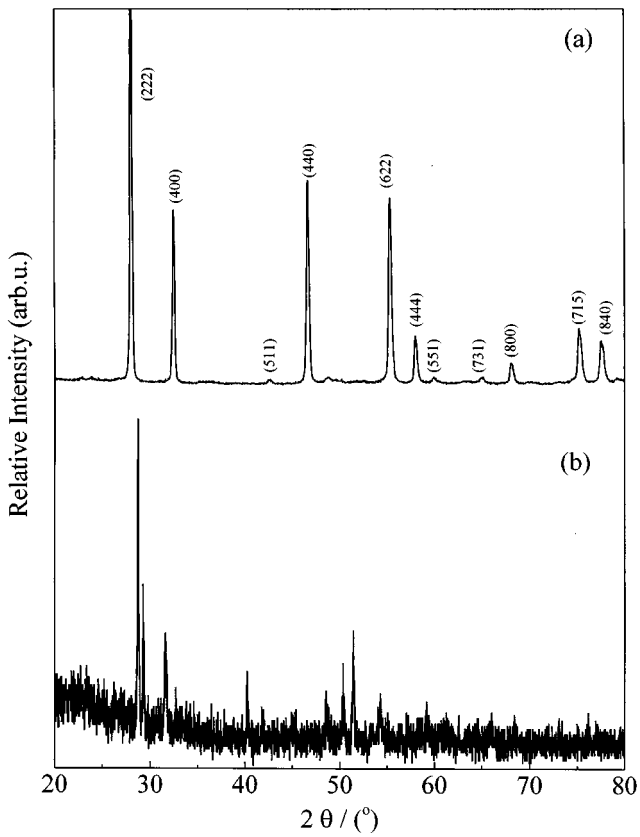

FIG. 1. XRD patterns for (a) $Bi_2Pb_2O_7$ under the present hydrothermal conditions and (b) a new phase after high-temperature treatment of $Bi_2Pb_2O_7$.

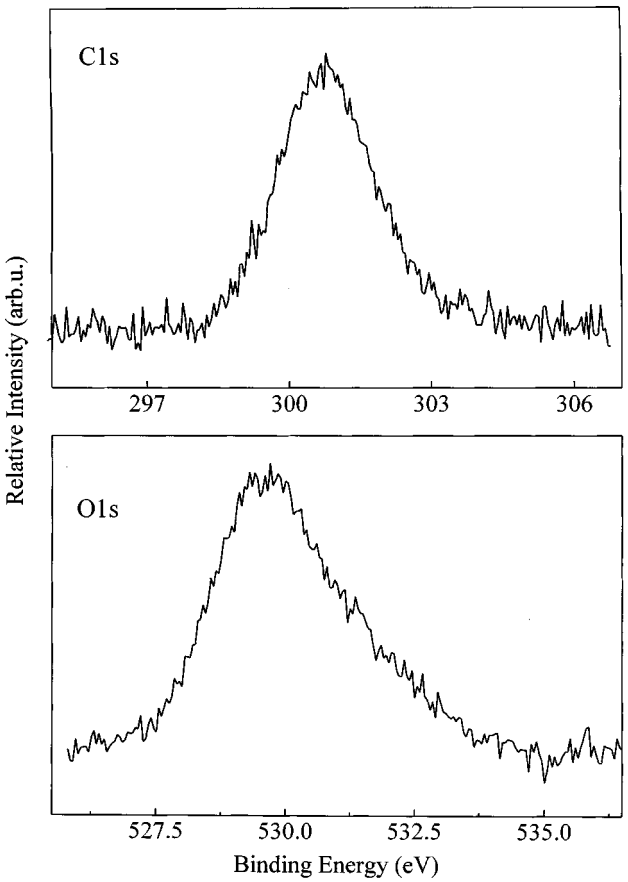

FIG. 2. C 1*s* and O 1*s* core-level spectra of $Bi_2Pb_2O_7$.

$4f_{7/2,5/2}$ peaks are highly symmetric. The energy positions are 158.5 eV for Bi $4f_{7/2}$ and 164.1 eV for Bi $4f_{5/2}$. This is in good agreement with our previous result on $(CeO_2)_{1-x}(BiO_{1.5})_x$ under hydrothermal conditions (18). In Fig. 3, peak asymmetry was not observed at either the lower binding energy or the higher binding energy of the Bi $4f_{7/2,5/2}$ peaks corresponding to Bi^0 or Bi^{5+}. Therefore, the bismuth ions were present as Bi^{3+} in the sample $Bi_2Pb_2O_7$.

The Pb 4*f* XPS spectrum of the sample $Bi_2Pb_2O_7$ is shown in Fig. 4. The same levels for $Pb^{4+}O_2$ and $Pb^{2+}O$ are also illustrated for comparison. The binding energy and the full width at half maximum of the Pb $4f_{7/2}$ peak for $Bi_2Pb_2O_7$ are 136.9 and 2.1 eV, respectively, and are consistent with those of the reference $Pb^{4+}O_2$. In addition, peak asymmetry was not observed at the higher binding energy of the Pb $4f_{7/2,5/2}$ peaks corresponding to Pb^{2+}, suggesting that there are only Pb^{4+} ions in our sample.

The formula for the pyrochlore type structure can be described as $A_2B_2O_7$, where the A-site cations with a larger ionic size occupy the eightfold coordination sites and the B-site cations with a smaller ionic size are distributed at distorted octahedral sites. Theoretically, for our sample $Bi_2Pb_2O_7$, different valences for Bi and Pb may yield two different products, $Bi_2^{3+}Pb_2^{4+}O_7$ or $Pb_2^{2+}Bi_2^{5+}O_7$, with different occupations. In fact, Bi^{3+} is the most stable oxidation state for bismuth in an oxygen lattice. Subramanian (18) has shown that Bi^{5+} is very difficult to stabilize in the sixfold coordinated states in the oxygen lattices due to a very large

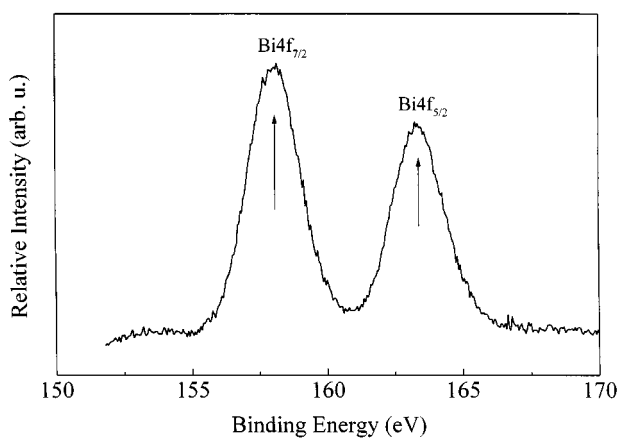

FIG. 3. Bi 4*f* core-level spectrum of $Bi_2Pb_2O_7$.

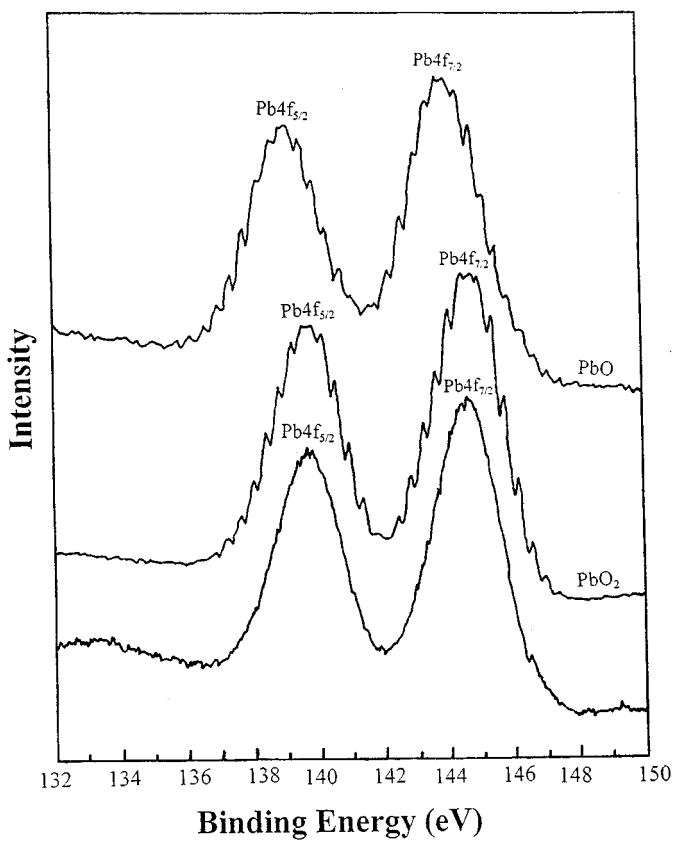

FIG. 4. Pb 4*f* core-level spectrum of $Bi_2Pb_2O_7$. The XPS spectra of $Pb^{2+}O$ and $Pb^{4+}O_2$ are also illustrated for comparison.

covalence in the Bi^{5+}–O bond needed for the stabilization of Bi^{5+}, the highest oxidation state for Bi. The oxidation of Bi^{3+} to Bi^{5+} can be achieved only under high oxygen pressures by the use of peroxides. On the basis of the above elemental analysis, valence determination, and structural considerations, we could describe the formula of our product as $Bi_2^{3+}Pb_2^{4+}O_7$.

4. *Thermal Stability of $Bi_2Pb_2O_7$*

Figure 5 shows the heating and subsequent cooling TG–DTA curves of $Bi_2Pb_2O_7$. The slight weight loss process observed below 380°C arises from the dehydration of the hydroxyl species absorbed on the sample surface. Above 450°C, ca. 3.2% weight loss was observed, which corresponds to one oxygen molecular release per formula unit of $Bi_2Pb_2O_7$. The weight never returned to the initial level during the cooling process. This weight loss corresponds to a complete reduction process from Pb^{4+} to Pb^{2+} in $Bi_2Pb_2O_7$, which may be caused by the transformation of $Bi_2Pb_2^{4+}O_7$ into $Bi_2Pb_2^{2+}O_5$ with liberation of O_2. This result also confirms our XPS identification of Bi^{3+} and Pb^{4+} for $Bi_2Pb_2O_7$. A similar reduction process from Pb^{4+} to Pb^{2+} has been found for $CaPbO_3$ with high temperature and pressure (20). However, the reduction process for our

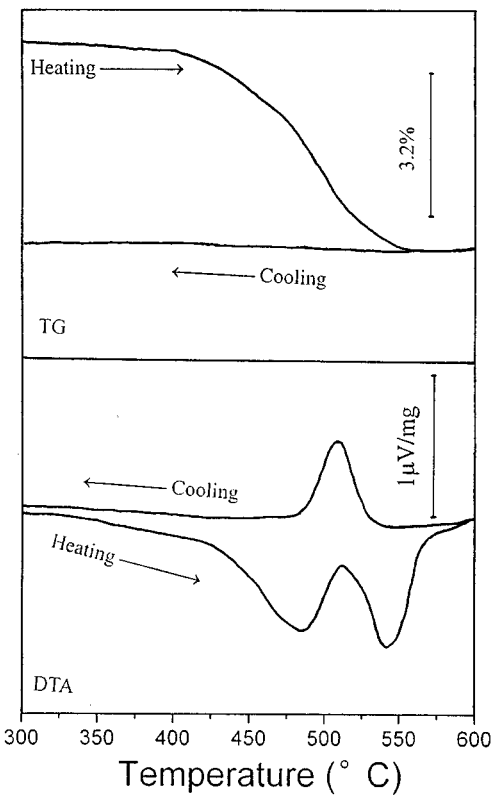

FIG. 5. Heating and subsequent cooling TG–DTA curves for $Bi_2Pb_2O_7$ in flowing O_2.

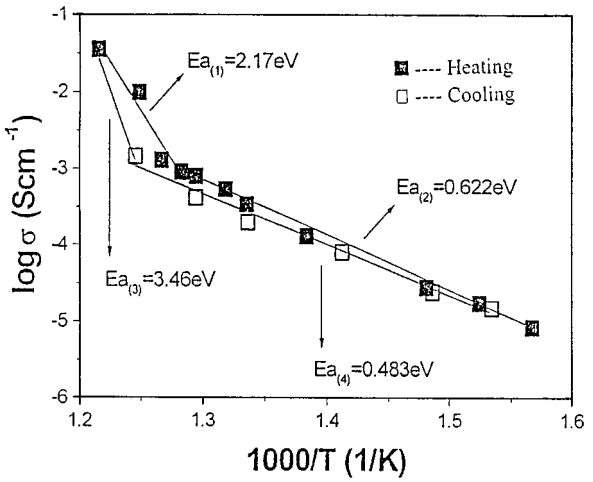

FIG. 6. Relationship of conductivity and temperature for $Bi_2Pb_2O_7$ during the heating and cooling processes.

$Bi_2Pb_2O_7$ may be more complex, as indicated by the two endothemic peaks observed in the corresponding temperature range. When the reduction process was complete, a new high-temperature phase was formed. This high temperature phase is metastable and will transform into another new phase. This is confirmed by an exothermic peak at 527°C with no weight loss occurring during the cooling process. The XRD pattern for the final product is shown in Fig. 1b. No component oxides, such as Bi_2O_3, PbO_2, or PbO, were found.

5. *Ionic Conduction of $Bi_2Pb_2O_7$*

The ionic conductivity of $Bi_2Pb_2O_7$ was measured in O_2 at different temperatures. Figure 6 shows the temperature dependence of the conductivity for $Bi_2Pb_2O_7$ during the heating and subsequent cooling processes. There was an onset in conductivity of $Bi_2Pb_2O_7$ at ca. 500°C (with a change in activation energy from 0.622 to 2.17 eV), corresponding to the formation of a new high-temperature phase. The high-temperature phase showed a high oxygen conductivity at relatively low temperature. Its conductivity reached 3.71×10^{-2} S cm^{-1} at 550°C. The discontinuity of the conductivity data occurring in the cooling process is associated with a phase transformation of the metastable phase into a stable phase under ambient conditions. This is in good agreement with our TG–DTA analysis.

CONCLUSIONS

A high-pressure phase $Bi_2Pb_2O_7$ was stabilized under mild hydrothermal conditions. A single-phase product can be obtained at crystallization temperatures varying from 140 to 240°C. $Bi_2Pb_2O_7$ is a metastable phase, which

transforms into a new phase at high temperature. The structural transformation is caused by a complete reduction from Pb^{4+} to Pb^{2+}. Its high-temperature phase showed promising oxygen conduction at high temperatures. This high-temperature phase will transform into a stable phase during the cooling process.

REFERENCES

1. T. Takahi and H. Iwahana, *Mater. Res. Bull.* **13,** 1447 (1978).
2. M. J. Verkerk and A. J. Burggraaf, *Solid State Ionics* **3/4,** 463 (1981).
3. V. G. Gattow and H. Fricke, *Z. Anorg. Allg. Chem.* **324,** 287 (1963).
4. M. A. Subramanian, A. K. Ganguli, and A. W. Seight, *Mater. Res. Bull.* **27,** 799 (1992).
5. C. J. Harlan, A. Kareiva, D. B. MacQueen, R. Cook, and A. R. Barron, *Adv. Mater.* **9,** 68 (1997).
6. J. Gopalakrishnan, *Chem. Mater.* **7,** 1265 (1995).
7. K. P. Reis, A. Ramanan, and M. S. Whittingham, *J. Solid State Chem.* **91,** 394 (1991).
8. H. Zhao and S. Feng, *Chem. Mater.* **11,** 958 (1999).
9. G. Li, S. Feng, L. Li, X. Li, and W. Jin, *Chem. Mater.* **9,** 2894 (1997).
10. G. Pang, S. Feng, Y. Tang, C. Tan, and R. Xu, *Chem. Mater.* **10,** 2446 (1998).
11. G. Li, L. Li, S. Feng, M. Wang, L. Zhang, and X. Yao, *Adv. Mater.* **146,** 11 (1999).
12. X. Xun, S. Feng, J. Wang, and R. Xu, *Chem. Mater.* **9,** 2966 (1997).
13. C. Zhao, S. Feng, Z. Chao, C. Shi, R. Xu, and J. Ni, *Chem. Commun.* **8,** 356 (1996).
14. K. Fueki, Y. Idemoto, and T. Yamauchi, *Physica C* **6,** 190 (1991).
15. B. G. Hyde, "Inorganic Crystal Structures." Wiley, New York, 1989.
16. N. Kumada, M. Hosoda, and N. Kinomura, *J. Solid State Chem.* **106,** 476 (1993).
17. H. Taguchi, A. Sugita, M. Nagao, and K. Tabata, *J. Solid State Chem.* **119,** 164, (1995).
18. G. Li, Y. Mao, L. Li, S. Feng, M. Wang, and X. Yao, *Chem. Mater*, **11,** 1259 (1999). [And references therein]
19. M. A. Subramanian, *Mater. Res. Bull.* **30,** 317 (1995).
20. A. Yamamoto, N. R. Khasanova, F. Izumi, X. J. Wu, T. Kamiyama, S. Torii, and S. Tajima, *Chem. Mater.* **11,** 747 (1999).